Electronic Supplementary Material (ESI) for Catalysis Science & Technology.
This journal is © The Royal Society of Chemistry 2020

Cu- and Fe-sites speciation in a composite zeolite catalyst for selective catalytic reduction of NO_x: insights from operando XAS

Ilia Pankin[a,b], Houeida Issa Hamoud[c], Kirill A. Lomachenko[d]*, Søren Birk Rasmussen[e], Andrea Martini[a,b], Philippe Bazin[c], Valentin Valtchev[c], Marco Daturi[c]*, Carlo Lamberti[a,b†], Silvia Bordiga[a,f]

(a) -Department of Chemistry, NIS Center and INSTM Reference Center, University of Turin, via P. Giuria 7, 10125, Turin, Italy
(b) Smart Materials, Research Institute, Southern Federal University, Sladkova Str. 174/28, 344090, Rostov-on-Don, Russia
(c) Laboratoire Catalyse & Spectrochimie, ENSICAEN - Université de Caen - CNRS 6 Boulevard Maréchal Juin, 14050 Caen, France
(d) European Synchrotron Radiation Facility, 71 Avenue des Martyrs, CS 40220 Grenoble Cedex 9, 38043, France
(e) Haldor Topsøe, Haldor Topsøes Allé 1, 2800 Lyngby, Denmark.
(f) Center for Materials Science and Nanotechnology (SMN), Department of Chemistry, University of Oslo, 1033 Blindern, 0315, Oslo, Norway

Supporting information.

Table of contents:

1 Catalytic data analysis and comparison with IR-conditions experiment.

Catalytic experiments made at the synchrotron were repeated in the laboratory with the same reactor-cell and similar pellet masses, in order to verify the coherence of the catalytic results. The Aabspec CXX 800 °C reactor cell was connected to a gas distribution and analysis system, described previously [1]. Prior to the experiment, the catalyst pellets were pretreated at 500 °C for 2 h with a temperature ramp rate of 5 °C/min under 10 % of O_2 in Ar. Then, the reaction was studied in the 450 °C and 150 °C temperature range using a model feed gas composition equivalent to that used at the synchrotron: 500 ppm NO + 500 ppm NH_3 + 10% O_2 + 2% H_2O in an Ar flow. The gas flow rate was controlled at 100 ml min^{-1}. All the reactants were stabilized before being sent to the cell and analysed by Mass Spectrometry (Quadrupole Pfeiffer Omnistar GSD 301), which also measured the output gas from the Aabspec CXX 800 ºC reactor-cell.

We can remark the excellent agreement between the results obtained during the *operando* XAS experiment at the synchrotron and at LCS laboratory (University of Caen), in the same conditions and pellet masses (See Figure 1 of the main text). However, one observes that the changes in the mass of the catalyst and total flow passing through the system yields essential difference in conversion activity with respect to our previous results collected upon *operando* IR experiments [1]. To account for different mass of the catalyst and total flow rate, the NO conversion was recalculated. First, the kinetic constants were calculated in accordance with following equation:

$$k = -\frac{F_{tot}}{W_{cat}}\ln(1-X) \quad (eq.S1)$$

where *k* is a kinetic constant, but normalized to weight; it comes out as mL reactant per weight, per time unit due to the first order of reaction for NO; F_{tot} is total (normal) flow in mL/s; W_{cat} is the mass of the catalysts and X is NO conversion measured as reported in *eq. S1*.

Once the kinetic constant calculated for every sample and experiment, it is possible to reversely calculate the conversion in a normalized situation, for example for the relevant GHSV of 50000 h^{-1}. The corresponding data is reported in Figure 1 of the main text and discussed in Section "Catalytic activity". At the same time we need to remark that the conversion rates are very high, so that we can estimate to be in the kinetic regime only for the low temperature range (T < 250 ºC), due to the fact that the sample mass was notably increased in order to maximize XAS signal. However, the conversion rates between the samples are preserved, so that we can confidently correlate the XAS with the catalytic results.

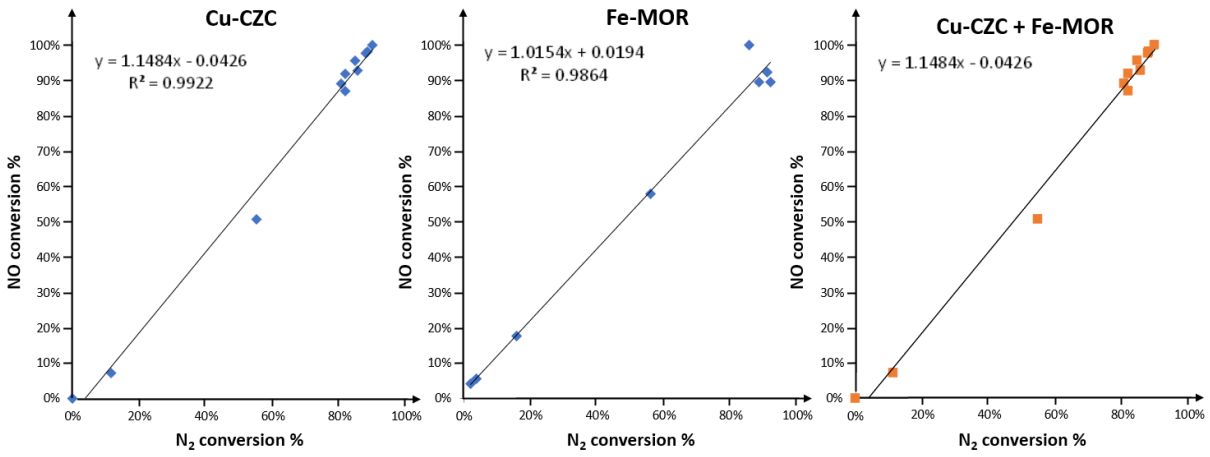

Figure S1 NO vs. N_2 conversion over Cu-CZC, Fe-MOR and mechanical mixture Cu-Fe-mix during XAS operando experiment.

Also, it should be mentioned that linear dependence of N_2 vs. NO conversion for the investigated samples as measured during XAS operando experiment (reported in Figure S**1**) assume that very small of N_2O is produced. Moreover, no N_2O was detected for investigated samples during the laboratory experiment (reported in our previous work [1]), where on-line IR cell analyzer was utilized known as the most sensitive technique for N_2O detection.

2 Preliminary XRD characterization.

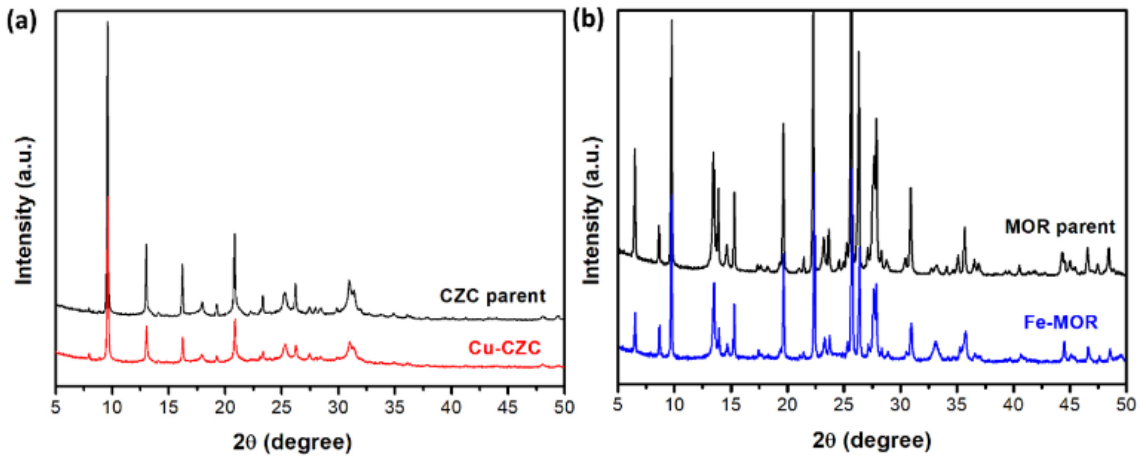

Figure S2. PXRD patterns collected for Cu/Fe exchanged and not exchanged **(a)** SAPO-34 and **(b)** MOR frameworks.

3 Fe K-edge EXAFS fitting

3.1 Fit parametrization details

Thanks to the good quality of the experimental signal the Fourier transformation for all Fe K-edge EXAFS data reported in the article has been performed for $k^2\chi(k)$ in the *k*-range from 2.8 $Å^{-1}$ to 14.1 $Å^{-1}$. EXAFS fitting has been performed in R space for k^2-weighted EXAFS amplitudes in the range from 1.1 to 3.5 Å, thereby capturing 2nd and 3rd peaks of Fourier transformed experimental signal.

All SS and MS paths contributions within the effective path lengths up to 4.2 Å has been accounted for the fit. Different SS and MS paths above the first two oxygen shells were parametrized by scaling coefficients *n1, n2* and *n3* intended to describe the CNs corresponded to the first (*n1*) and higher coordination shells (*n2, n3*). Atomic displacement and DW (Debye-Waller) factors of the first two oxygen shells were parametrized independently and reported as $\Delta R\_O_{1/2}$ and $\sigma^2\_O_{1/2}$, respectively. While the atomic displacement of more distant atoms starting from the first Fe-Fe coordination shell, were parametrized by unified scaling coefficient α. The corresponding DW factors for the paths atomic scatters beyond the first two oxygen shells were parametrized on the basis of the proportionality of the square root in accordance with the ratio of the distances by $\sigma_i = \sigma_{far}(Ri/R_{reff})^{1/2}$ [2, 3], where R_i corresponds to effective lengths of the current scattering path, while R_{reff} (2.89 Å) is the effective length for the first Fe-Fe coordination shell SS path (actually represented by a single Fe at the distance ~ 2.89 Å) parametrized solely by σ_{far}. It is also worth to emphasize, that all MS paths included in the fit were parametrized by the product of different CNs scaling coefficient, in accordance with the "affiliation" of the scatterers to a particular coordination shell (*e.g.* if the MS path is consist of the atomic sites which individual SS paths parametrized by *n1* and *n3* coefficients, the corresponding passive amplitude reduction factor will be parametrized by the product $S_0^2 n1n3$; such parametrization roughly gives a meaning of occupancy for scaling coefficient *n1, n2, n3* when it is employed for MS paths and allow to get lower R-factor with respect to the fits where MS paths were parametrized by a single CNs scaling coefficient).

Almost for all fits one or two correlations above 0.9 were obtained (See Table S**2**, Table S**3** and Table 2 of the main text). We aware by this fact, however fixing some of the correlated parameters the fit remained stable and yields very similar results. So, there is no way to avoid these undesirable correlations that are present in the fit, likely because of large number of scattering paths included in the fit. Considering a limited number of independent variables within the selected fit range, we were obliged to find a compromise parametrizing a large number of scattering paths by the limited number of variables parameters.

For the dataset collected under SCR condition in a wide temperature range the multi-dataset fit with DWFs parametrized in accordance with Einstein model [4, 5] has been performed (See Figure S**4**b) in addition to the standard fit (See Figure S**4**a and Table S**4**). The Einstein model approximates the vibrational density of states as a Dirac delta function spiked at a single frequency, so called Einstein frequency (ω_E). Under this approximation, the DWFs behavior for multiple dataset (collected at different temperatures) is determined by the only one parameter – Einstein temperature (θ_E)– in accordance with following expression:

$$\sigma_X^2(T) = \frac{\hbar^2}{2\mu k_B \theta_E^X} \coth\left(\frac{\theta_E^X}{2T}\right) \qquad (eq.\ S2)$$

where θ_E the Einstein temperature, related with the Einstein frequency (ω_E) by the relationship: $\hbar\omega_E = k_B\theta_E$, where ħ = 1.055 10^{-34} J s - is the reduced Plank constant and k_B = 1.38 x 10^{-23} K^{-1} - is the Boltzmann constant. The rest of the parametrization is similar to the single dataset fit parametrization described above. The best fit for the multiple datasets composed by all 9 temperature point measurements yields Einstein temperature θ_E = 333.01 ºC.

Importantly that despite the multi-dataset character of the fit some of the guess parameters (E_o and α) were refined independently for each temperature point. As expected, the multi-dataset fit yields higher R-factor with respect to the independent fit of the dataset for each temperature point, however an overall fit quality (See Figure S**4**b) is still good and confirm the structure of α-Fe_2O_3 oxide as an initial guess.

3.2 Additional fit results.

Table S1 reports coordination numbers as refined for α-Fe_2O_3 (hematite), Fe-MOR and Cu-Fe-mix samples at RT recalculated from the corresponding scaling coefficients *n1, n2, n3* reported in Table 2 of the main text. Only few strongest SS path that contribute to the intensity of the 1st, 2nd and 3rd EXAFS peaks are reported in the table. Coloumn "init. CN's" and "init. R" corresponds to the the distances and coordination numbers taken from initial guess structure of α-Fe_2O_3 [29] (American Mineralogist database, str. № 0000143).

Coeff. / SS path		Init. R, Å	Init. CN's	**α-Fe_2O_3**	**Fe-MOR**	**Cu-Fe-mix**
n1	O_1	1.946	3.0	**2.76**±0.18	**2.79**±0.15	**2.76**±0.15
	O_2	2.116	3.0	**2.76**±0.18	**2.79**±0.15	**2.76**±0.15
n2	Fe_1	2.899	1.0	**1.02**±0.06	**0.78**±0.07	**0.79**±0.06
	Fe_2	2.971	3.0	**3.06**±0.18	**2.34**±0.21	**2.37**±0.18
n3	Fe_3	3.364	3.0	**2.52**±0.30	**1.41**±0.27	**1.47**±0.27
	O_3	3.398	3.0	**2.52**±0.30	**1.41**±0.27	**1.47**±0.27
	O_4	3.597	3.0	**2.52**±0.30	**1.41**±0.27	**1.47**±0.27
	Fe_6	3.705	6.0	**5.04**±0.60	**2.82**±0.54	**2.94**±0.54

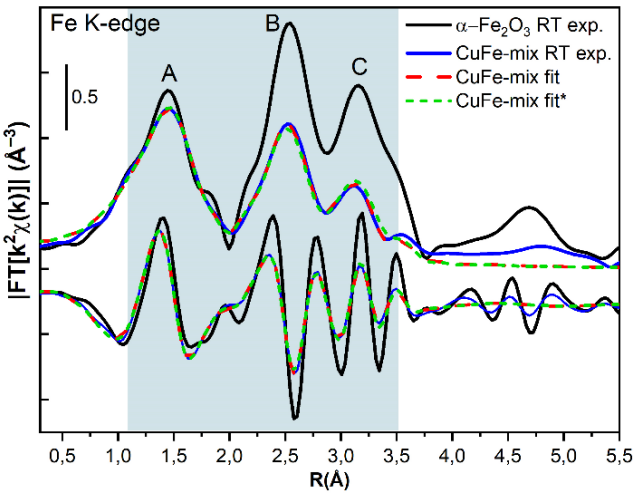

Figure S3 Fe K-edge k^2-weighted EXAFS phase uncorrected amplitudes (upper curves) and corresponding imaginary parts (bottom curves) collected for bulk oxide phase α-Fe_2O_3 at RT and Cu-Fe-mixed at RT before activation. Dashed red and dotted green lines demonstrate the best fit obtained by the standard fit procedure and fit where CNs were parametrazed by equation (eq.2) in order to evaluate cluster size, respectively. Blue rectangle area represents the fit range in R-space.

Table S2 The fit results reported for k^2-weighted EXAFS amplitudes obtained for bulk oxide phase α-Fe_2O_3 as well as Fe-MOR and Cu-Fe-mix at RT. The variables that has been fixed upon fit procedure is underlined. * The fit results were obtained by using special approach for parametrization of CNs in accordance with equation (*eq. 2*) from the main text and reported elsewhere [6, 7]. $n1$, $n2$ and $n3$ coefficients reported for Fe-MOR* fit were fixed as obtained for α-Fe_2O_3 and represent N_i^{bulk}. An averaged cluster size <D> obtained within this approach is reported also in Table 2 of the main text. N_{ind} and N_v corresponds to the number of independent and variable parameters.

Fit parameters	**α-Fe_2O_3**	**Fe-MOR***	**Cu-Fe-mix***
ΔE (eV)	-4.03 ± 0.45	-2.96 ± 0.47	-2.39 ± 0.44
N_{ind}/N_v	17.6 / 11	17.6 / 8	17.6 / 8
S_0^2	0.799	0.799	0.799
R-factor	0.0030216	0.0045455	0.0040163
n_1	0.92 ± 0.06	0.92	0.92
n_2	1.02 ± 0.06	1.02	1.02
n_3	0.84 ± 0.010	0.84	0.84
ΔR_O_1 (Å)	-0.015±0.005	-0.022± 0.007	-0.022±0.007
ΔR_O_2 (Å)	-0.029±0.008	-0.051±0.009	-0.051±0.009
α (Å)	-0.0046±0.0025	-0.0006 ± 0.0033	-0.0001± 0.0031
σ^2_O_1 (Å^2)	0.0015±0.0008	0.0043 ± 0.0009	0.0044±0.0009
σ^2_O_2 (Å^2)	0.0027± 0.0012	0.0060 ± 0.0014	0.0061± 0.0014
σ^2_far (Å^2)	0.0025± 0.0004	0.0056 ± 0.0006	0.0058± 0.0006
<D> (nm.)	n/d	2.2 ± 0.7	2.2 ± 0.8
highest correlations	no correlations higher than 0.90	σ^2_far/<D>=0.932	<D>/σ^2_far = 0.931

Table S3 The fit results reported for k^2-weighted EXAFS amplitudes obtained for Cu-Fe-mixed sample at steady-state conditions at RT, 200 ºC and 500 ºC upon activation. The independent single dataset fit was performed for each temperature. The variables that has been fixed upon fit procedure are underlined. The fit results obtained for RT is also reported in Table 2 of the main text. N_{ind} and N_v corresponds to the number of independent and variable parameters.

Fit parameters	**Cu-Fe-mix**		
	RT	**200 ºC**	**500 ºC**
ΔE (eV)	-2.34 ± 0.40	-3.24 ± 0.41	-3.02 ± 0.50
N_{ind}/N_v	17.6 / 10	17.6 / 7	17.6 / 7
S_0^2	0.799	0.799	0.799
R-factor	0.0024579	0.0033186	0.0040716
n_1	**0.92**±0.05	**0.92**±0.05	**0.92**±0.05
n_2	**0.79**±0.06	**0.79**±0.06	**0.79**±0.06
n_3	**0.49**±0.09	**0.49**±0.09	**0.49**±0.09
ΔR_O_1 (Å)	-0.021±0.007	-0.030±0.010	-0.008±0.012
ΔR_O_2 (Å)	-0.051±0.009	-0.071± 0.012	-0.072±0.025
α (Å)	-0.0008±0.003	-0.0015± 0.003	0.0099±0.005
σ^2_O_1 (Å^2)	0.0043± 0.0011	0.0068±0.0011	0.0094±0.0010
σ^2_O_2 (Å^2)	0.0061±0.0018	0.0095±0.0022	0.0208± 0.0043
σ^2_far (Å^2)	0.0054±0.0006	0.0076±0.0002	0.0117± 0.0003
<D> (Å)	n/d	n/d	n/d
highest correlations	no correlations higher than 0.90	σ^2_O_2/ΔR_O_1 = 0.928	σ^2_O_2/ΔR_O_1 = 0.913

Table S4 The fit results reported for k^2-weighted FT-EXAFS amplitudes obtained for Cu-Fe-mixed sample under NH_3-SCR conditions in a wide temperature range. The CNs coefficients (*n1*, *n2* and *n3*) and S_0^2 have been fixed as refined for activated sample, See Table S**3**.

Parameters	**Cu-Fe-mix sample**							
	100 ºC	**150 ºC**	**200 ºC**	**250 ºC**	**300 ºC**	**350 ºC**	**400 ºC**	**450 ºC**
ΔE (eV)	-3.00±0.37	-2.68±0.38	-2.72±0.39	-2.57±0.48	-2.83±0.42	-2.99±0.50	-3.23±0.49	-2.74±0.48
N_1/N_v	17.6 / 7	17.6 / 7	17.6 / 7	17.6 / 7	17.6 / 7	17.6 / 7	17.6 / 7	17.6 / 7
R-factor	0.0030	0.0034	0.0035	0.0044	0.0034	0.0034	0.0034	0.0039
Reduced χ^2	67.132	132.820	124.578	147.464	82.477	82.477	105.763	112.079
ΔR_O_1 (Å)	-0.019±0.008	-0.021±0.008	-0.022±0.009	-0.012±0.013	-0.010±0.013	-0.008±0.015	-0.006±0.014	-0.005±0.012
ΔR_O_2 (Å)	-0.058±0.011	0.058±0.011	0.058±0.012	0.062±0.018	-0.068±0.018	-0.068±0.022	-0.083±0.025	-0.071±0.024
α (Å)	0.0010±0.0028	0.0011±0.0031	0.0022±0.0032	0.0047±0.0041	0.0048±0.0037	0.0059±0.0044	0.0042±0.0042	0.0092±0.0045
$\sigma^2\_O_1$ (Å^2)	0.0057±0.0009	0.0058±0.0009	0.0061±0.0009	0.0073±0.0011	0.0081±0.0010	0.0084±0.0011	0.0093±0.0011	0.0091±0.0010
$\sigma^2\_O_2$ (Å^2)	0.0096±0.0020	0.0100±0.0021	0.0109±0.0022	0.0138±0.0037	0.0153±0.0037	0.0166±0.0043	0.0186±0.0042	0.0199±0.0042
σ^2_far (Å^2)	0.0061±0.0002	0.0069±0.0002	0.0075±0.0002	0.0082±0.0003	0.0089±0.0002	0.0096±0.0003	0.0103±0.0003	0.0110±0.0003
highest correlations	no correlations > 0.9	no correlations > 0.9	no correlations > 0.9	$\sigma^2\_O_2$ / ΔR_O_1 = 0.94	$\sigma^2\_O_2$ / ΔR_O_1 = 0.94	$\sigma^2\_O_2$ / ΔR_O_1 = 0.94	$\sigma^2\_O_2$ / ΔR_O_1 = 0.92	$\sigma^2\_O_2$ / ΔR_O_1 = 0.91

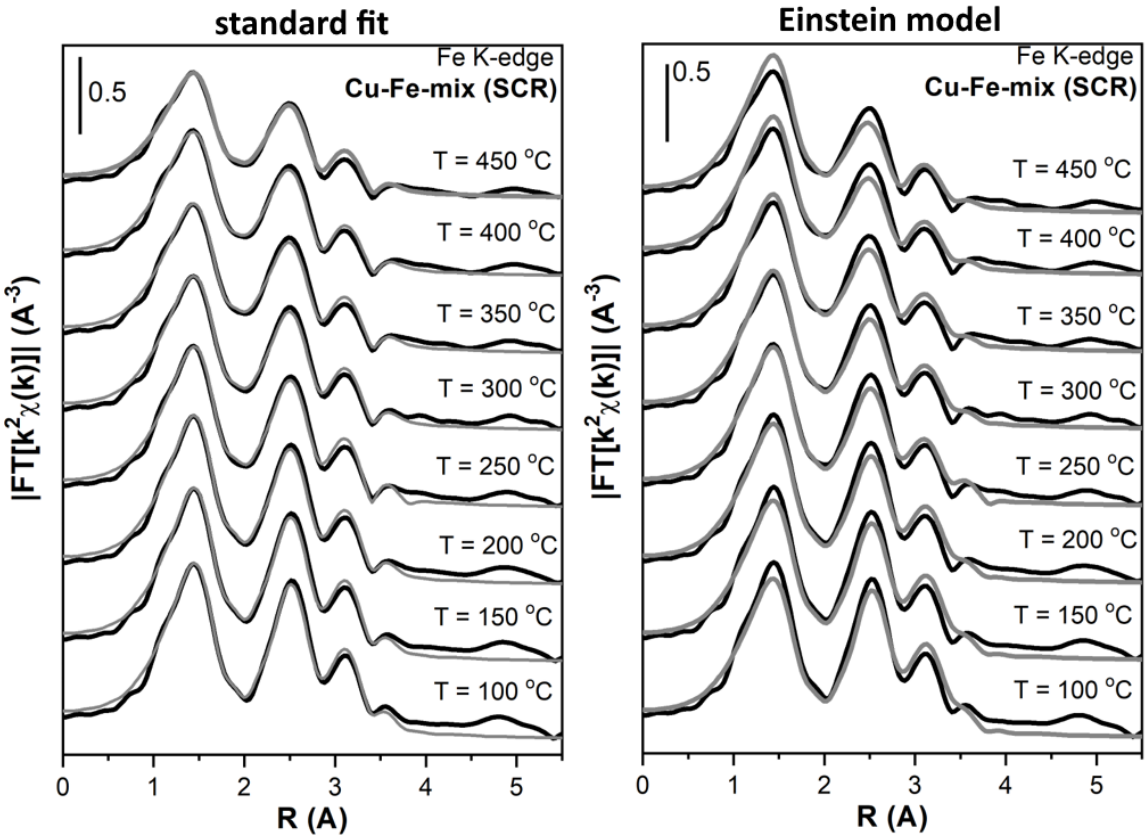

Figure S4 Comparison of the EXAFS fit results obtained for Cu-Fe-mix dataset collected under NH_3-SCR conditions in a wide temperature range **(a)** by single-datset fit for each temperature point and **(b)** by multi-dataset fit implementing Einstein model for DWFs parametrization. For both cases, the coordination number scaling coefficients has been fixed as obtained for RT fit. For more details see Section 3.1.

4 Fe K-edge differential XANES

The differential XANES signal obtained as a difference between Fe-MOR minus Cu-Fe-mix sample. First, we will analyze the differential XANES signal for the activated samples shown as a purple dashed line in Figure S**5**. The comparison of the energy localization for the features obtained for differential XANES signal with respect to the normalized μ(E) XANES signal of Fe-MOR (collected at 150 ^{o}C under SCR conditions and reported as a dotted black curve at Figure S**5** for clarity) show that features B and B* (located at ~ 7121 eV and ~ 7125 eV, respectively) observed for the differential XANES spectra can be caused by the energy shift of absorption threshold. As it was discussed in the main text the tiny energy shift observed for the samples under high T activation can be associated with temperature-induced structural rearrangements, that likely should be more pronounced for surface Fe sites of the small Fe_2O_3 clusters or for minority of the isolated Fe species. The similar shape of the differential XANES signal (with respect to the difference obtained for the activated samples) has been also obtained for low temperature dataset acquired under NH_3-SCR conditions, resulting to even slightly more pronounced negative features B and B* and positive peaks C and C* (located at 7134 eV ~ and ~ 7138 eV, respectively).

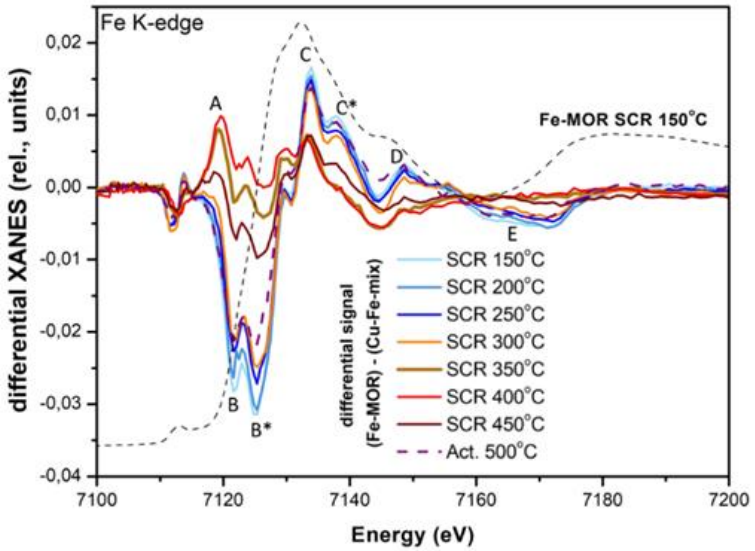

Figure S5. Fe K-edge differential XANES spectra obtained as a difference between Fe-MOR and Cu-Fe-mixed XANES spectra acquired under NH_3-SCR conditions at different temperatures. Purple dashed line corresponds to the differential XANES obtained for the activated samples at 500 ^{o}C. Dashed grey curve correspond to the normalized Fe K-edge XANES spectra collected at 150 ^{o}C shown here for easier interpretation of the differential XANES features.

The interpretation of features B and B* as well as C and C* in differential Fe K-edge XANES indeed could be assigned with some temperature-induced structural rearrangements, however, quantitative EXAFS analysis reported above reveals structural similarity of small iron oxide clusters (particularly very similar cluster size, Fe-O distances and DW factors of oxygen species in the first coordination shell), both upon activation ramp and reaction conditions. Moreover, starting from the temperature of 350 ^{o}C and upwards, the shape of differential XANES spectra undergoes a dramatic changes that results to the formation of the positive peak A (located at around 7120 eV, in the area of the main adsorption threshold onset) and to the significant decrease of B, B* and C, C* features intensity, thus resulting to the damping of differential XANES signal.

5 PCA and statistical analysis of XANES

5.1 Cu K-edge dataset

The determination of the optimal number of principal components (PCs) is of crucial importance for the further LCF analysis reported in the main text of the article (for Cu K-edge dataset). In this work the determination of the PCs is performed on the basis of advanced statistical analysis as implemented in the recently released PyFitit package [8].

First, XANES dataset composed by 32 spectra acquired during the entire SCR-process, was constructed. The constituted data matrix (characterized by 87 energy points, from 8975 to 9020 eV) has been subjected to the singular value decomposition (SVD) procedure [9, 10]. From this technique, the eigenvectors (abstract components and their related eigenvalues) of the correlation matrix associated to the input XANES dataset were identified (Figure S**6**). The first abstract component represents principal components (PCs) that represents the directions of a X-dimensional space able to take account for the highest variance of the data, noise included. Each eigenvector is constituted by 87 points and, for this reason, can be considered as a spectrum but without a chemical/physical meaning, as it shown in Figure S**6**. For this reason, the eigenvectors of the correlation matrix are typically called "abstract spectra" or "abstract components" [11].

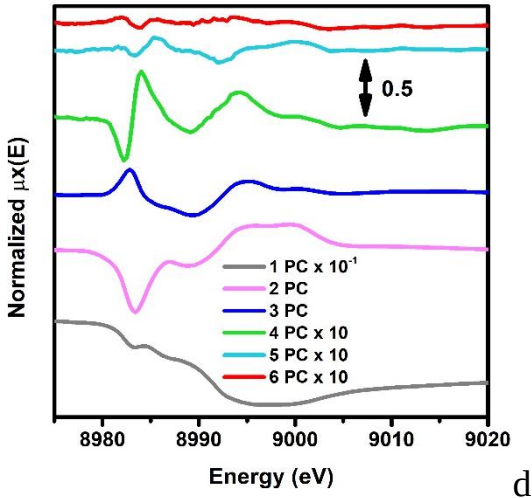

Figure S6 First six abstract spectra extracted from the covariance matrix associated to the Cu-CZC dataset acquired under the NH_3-SCR condition.

The eigenvalues of the correlation matrix represent, from a statistical point of view, the importance that each abstract component has in the data representation [10]. In order to identify the correct number of PCs able to represent the real/physical signal and not the noise and then the pure species associated to determined complexes in the mixture, different statistical criteria can be applied. In our analysis, we applied the most widely used techniques in the field of spectral mixture resolution such as: *Scree plot*, *IE* and *IND* values analysis and finally the *Fisher (F)-test* [10, 12]. The results of these test applied on the Cu-CZC reported in Figure S**7** (a-d).

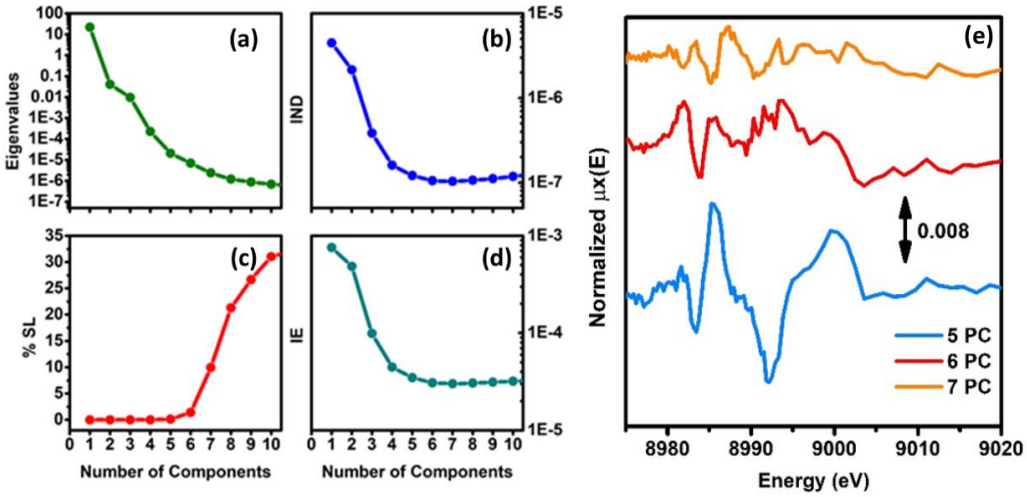

Figure S7 (a) Scree Plot, **(b)** IND plot, **(c)** %SL plot associated to the F-test, **(d)** IE plot related to the Cu-Fe mixed sample dataset acquired during the SCR condition. **(e)** Graphical representation of the fifth, sixth and seventh PCs associated to the Cu-CZC dataset acquired during the SCR condition. The fifth and sixth PCs are reported in Figure S5 as well.

The identification of the signal-related PCs comes directly from the analysis of each abstract spectra reported in Figure S**6**. The first four components are undoubtedly associated to the real signal; on the contrary, PC 5 and PC 6 are more dubious. However, if we compare them (See FigureS**7**e), it is possible to see that some defined features emerge in the fifth component while components sixth and seventh are predominantly dominated by noisy features, apart the peak appearing at ca.8983.8 eV in the sixth PC that can be associated to Cu species forming during a transient phenomenon. Taking into account all the above consideration it was concluded that the optimal number of PCs is 5 both for Cu-CZC and Cu-Fe-mix datasets (the analysis for Cu-Fe-mix dataset case is not reported for brevity).

As it was announced before, the abstract spectra reported in Figure S**6** and Figure S**7**e do not have chemical/physical meaning. However, different methods have been employed in order to recover some pure spectra and their related concentration profiles having a physical/chemical meaning. An example of successful implementation of Multivariate Curve Resolution (MCR) approach [13, 14] reported in few recent works [15, 16]. However, for the present case the algorithm of the physical/chemical meaningful XANES references based on the earlier successfully employed approach SIMPLISMA [17] has failed. Due to this fact for the further analysis standard linear combination fit routine has been employed. The results and motivation of selection of the spectra employed as a reference for LCF is reported in the Section S6.

5.2 Fe K-edge datdaset

For the Fe K-edge analysis, the XANES dataset was composed by 44 spectra acquired for only monometallic Fe-MOR sample both under activation and SCR conditions (for Cu-Fe-mixed sample the temperature evolution were monitored solely by Cu K-edge XANES, cause it is demonstrated significantly higher variations). The constituted data matrix (characterized by 164 energy points) has been subjected to the SVD procedure.

The different statistical criteria IND and Fisher Test (with a significance level fixed to 5%) proposed 6 and 4 PCs, respectively. (the XANES acquisition dataset of Fe-MOR sample used for analysis reported in Figure S16). The obtained abstract components are reported in Figure S**8**.

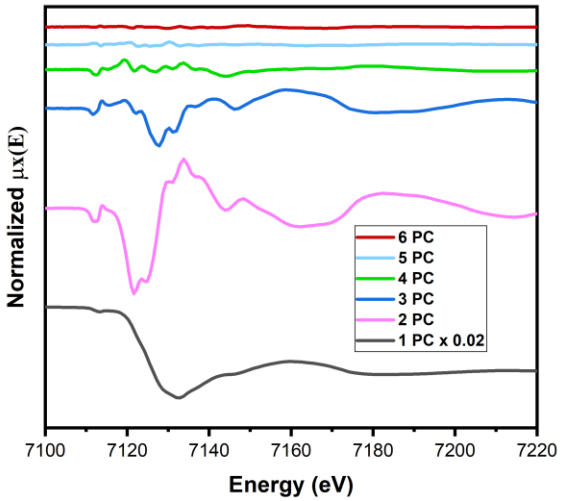

Figure S8 First six abstract component extracted from the covariance matrix associated to the Fe-MOR dataset acquired under high-temperature pretreatment and NH_3-SCR condition.

The first abstract component is close to the reverse average associated to the entire XANES dataset, appearing very similar to the one reported in Figure 2 of the main text or Figure S13 of SI. While the 2nd and 3rd are an additive to the 1st abstract component that allow accurate reproducing of each spectra from the investigated dataset. The 4th abstract component in principle also might have some physical/chemical meaning but its contribution is already dramatically small. While starting from the 5th abstract component they are on the level of noise. Considering that relatively intensive 2nd and 3rd abstract components in principle have a meaning of differential XANES spectra, thus they can be qualitatively compared with differential XANES signal as reported in Figure S**9**.

Indeed, one can see that shape of the 2nd and 3rd abstract components coincide well with experimental differential Fe K-edge XANES signal obtained as a temperature induced difference within Fe-MOR sample and as a difference between Fe-MOR and Cu-Fe-mix upon high-T pretreatment (See Figure S**9**). Thus, the obtained abstract component can describe experimentally observed differential XANES signal.

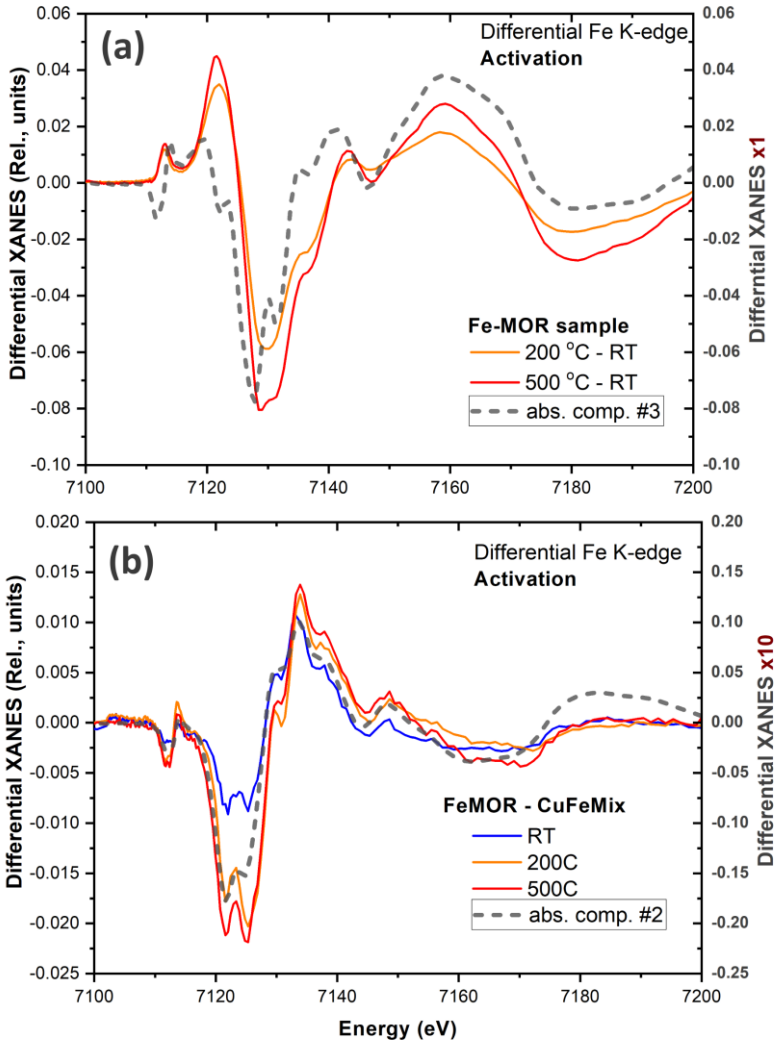

Figure S9 Comparison of the abstract component derived from statistical analysis of Fe-MOR dataset with differential Fe K-edge XANES signal obtained as **(a)** temperature induced difference within Fe-MOR sample and **(b)** difference between Fe-MOR and Cu-Fe-mix sample upon high temperature pre-treatment of the catalysts.

Accounting for the fact that statistical analysis showed that up to four abstract components might have physical/chemical meaning and for the similarity of the EXAFS fit results obtained for corresponding datasets we can assume that some of this components can be associated with the signal steaming from the minority of isolated iron species.

6 PCs selection and motivation for Cu K-edge dataset

Based on the statistical analysis of the Cu K-edge XANES dataset acquired under reaction conditions we used five pure components for LCF analysis of both monometallic Cu-CZC and bimetallic Cu-Fe-mixed samples in the entire temperature range. Description of the species is given in Table **5** and the corresponding spectra are shown in Figure S**10**.

Table S5 Cu-species selected as references for linear combination fit (LCF) analysis of operando XANES

Cu-type	***Z-Cu(II)***		***m-Cu(II)***	***m-Cu(I)***	
(Dominant) Cu-species	**$Cu^{II}(OH)/O_2$**	**$Cu^{II}(NO_3)$**	**$Cu(II)(NH_3)_3X$**	**$Cu^{I}(NH_3)_2$**	**$Cu^{I}(NH_3)O_{fw}$**
XAS data collection conditions	Cu CZC, 10%O_2 500 °C	Cu-Fe mix, 500 ppm NO + 10%O_2 (pre-treatment 500 ppm NO + 500 ppm NH_3) 200 °C	Cu-CHA (Si/Al=15, Cu/Al=0.5), 1000 ppm NO + 1200 ppm NH_3 (pre-treatment 10% O_2 + 1000 ppm NO), 50 °C	Cu-Fe mix, 500 ppm NO + 500 ppm NH3, 200 °C	Cu-CHA, (Si/Al=13, Cu/Al=0.44), MCR ALS component
Bibliographic references	[18]	[19],[20]	[21],[16]	[19], [22]	[16], [22]

Several changes were introduced in the set of the pure species compared to the original work of Lomachenko et al. [23]. First, accounting for recent experimental [16, 21] and theoretical [24] findings and considering the notable energy shift for the rising-edge feature upon temperature decrease under SCR conditions we have taken into account additional configuration for the quasi-linear amino complex $Cu^{I}(NH_3)O_{fw}$. In this configuration Cu(I) ion is coordinated by NH_3 that is pointing to the center of the cavity and by O_{fw} from the zeolite framework as reported by Giordanino et al., [22]. It was not possible to re-create experimental conditions where this complex is dominant species, because it always co-existed with the linear diammino $Cu^{I}(NH_3)_2$. Therefore, instead of the experimental spectrum we used a theoretical curve obtained by MCR ALS procedure from the dataset originating from NH_3 TPD experiment with Cu-CHA sample reported by Borfecchia et al. [16]. To further validate the structural assignment of the experimental XANES, derived by MCR approach in ref. [16], we report comparison of the XANES spectra simulated both mobile di-amino complex and framework coordinated $Cu^{I}(NH_3)O_{fw}$ (See Figure S**10**) [30]. XANES simulations has been performed on the basis of molecular orbitals approach as implemented in ADF package [25]. More details on XANES simulations is reported in our previous works [15, 18]. From Figure S**10** (a and b) one can see that the simulated XANES accurately reproduce the difference observed for two experimental XANES principal component associated with two different Cu^{I} complexes: (i) the energy shift of the rising-edge Cu(I) fingerprint feature, (ii) less deep character of the subsequent minima and (iii) the energy shift of

the second absorption peak towards the lower energy was obtained for $Cu^{I}(NH_3)O_{fw}$ with respect to mobile m-$Cu^{I}(NH_3)_2$.

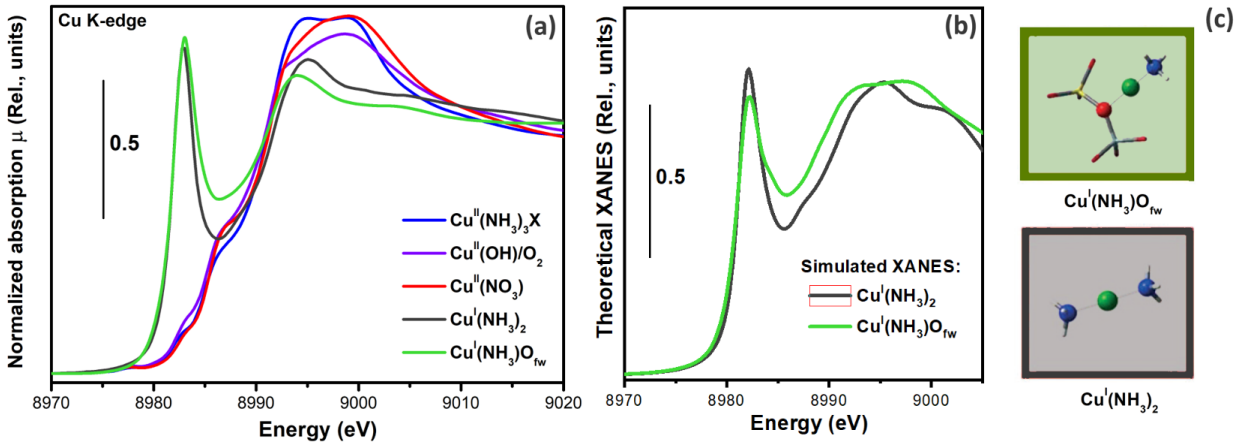

Figure S10 (a) Experimental XANES spectra of the 5 pure components used for linear combination fit of the entire XANES dataset collected under NH_3-SCR reaction for both monometallic (Cu-CZC) and bimetallic (Cu-Fe-mix) catalysts. **(b)** XANES simulations performed for linear m-$Cu^{I}(NH_3)_2$ and framework coordinated $Cu^{I}(NH_3)_2O_{fw}$ complexes reported to emphasize the necessity to account for two different Cu^{I} component for LCF analysis and their structural assignment reported at panel **(c).** green, blue and red spheres correspond to Cu, N and $O_{fw,}$ while the rest of the framework and hydrogen sites are shown as sticks. Panel (b) is adapted from Ref [30].

Then, tetra-ammino complex $Cu^{II}(NH_3)_4$ employed as independent component in the previous work was substituted by mixed-ligand complex that has been found to be formed upon exposure by NO/NH_3 feed after equilibration in NO/O_2 flux [21] (denoted as $Cu(NH_3)_3X$ in this work). This choice is justified by the fact that the experimental conditions for collecting this spectrum are much more relevant to SCR compared to those for $Cu^{II}(NH_3)_4$. Indeed, the latter was measured in solution, and the spectral shape was reported to be heavily influenced by the hydration shell [26]. Finally, the hydrated $Cu(H_2O)_6$ species were excluded from the fit, because the contribution was found to be small and unstable. At the same time, its inclusion as a 6^{th} component did not lead to significant improvement of the R-factor.

7 An extended results of Cu K-edge LCF analysis

The results of XANES linear combination fit analysis (LCF) for monometallic Cu-CZC and bimetallic Cu-Fe-mix samples are summarized in Figure S**11** . The top part of the figure i.e. panel (a) and (b) represent the temperature evolution profile for the 5 PCs described in detail in Section S6. The color code of the abundancy profiles are in correspondence with the spectra of PCs used for LCF analysis (shown in Figure S**10**). The vertical bars represent error bars for the abundancy values derived from XANES LCF. The bottom part of the Figure S**11** is duplicated from the main text (See Figure **7**) of the article and represent the temperature profile where the contributions from two framework coordinated complexes $Cu^{II}(NO_3)$ and $Cu^{II}(OH)/O_2$ are unified as Z-Cu(II) (red bars), while contribution from two Cu(I) species $Cu^{I}(NH_3)_2$ and $Cu^{I}(NH_3)O_{fw}$ are unified as Cu(I) (grey bars). The contribution from mobile mixed-ligand complex $Cu^{II}(NH_3)_3X$ reported as m-Cu(II). Panel (c) and (d) duplicate the results reported in the main text.

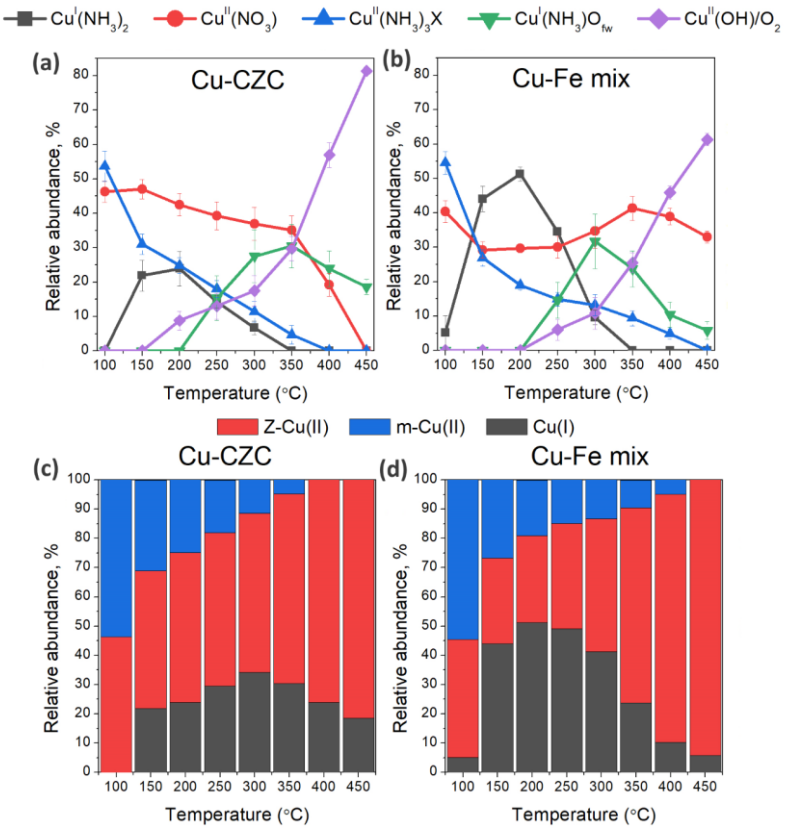

Figure S11 (a) and **(b)** relative abundance temperature profile for different Cu-species formed in the monometallic and bimetallic catalysts, respectively, under NH_3-SCR conditions, derived by XANES linear combination fit acconting for the 5 principle components. **(c)** and **(d)** the same results of the linear combination fit analysis presented in a way, where two different framework coordinated Cu^{II} and two different mobile Cu^{I} components were combined and reported as Z-Cu(II) and Cu(I), while the mobile Cu^{II} reported as m-Cu(II) for the sake of simplifcation. Panel **(c)** and **(d)** are also reported in the main text of the article.

8 Similarity of Cu-speciation in the activated samples.

Figure S**12** reports Cu K-edge XANES spectra and FT-EXAFS amplitudes collected at 500 ^{o}C for monometallic and bimetallic catalyst after high-temperature activation in oxidative conditions. The only notable differences in XANES is observed in the region of Cu(I) rising-edge feature (*ca.* 8983 eV), where monometallic catalyst show slightly more intensive shoulder, that can be interpreted by the minor presence of the self-reduced framework interacting Cu^{I} sites in Cu-CZC sample. The corresponding EXAFS amplitudes reported in the inset of Figure S**12** declare some differences in the intensity of the first shell peak, that stemming from possibly slightly different relative abundancy of three-fold or four-fold coordinated Cu-oxo species in the activated samples [27, 28].

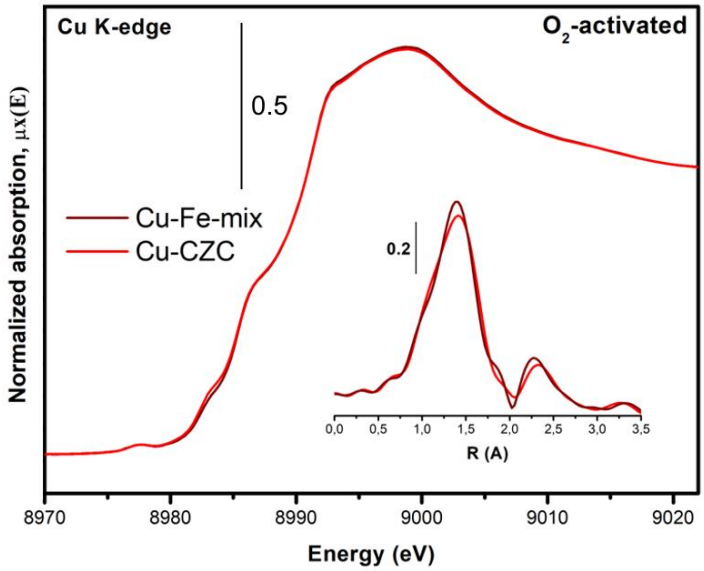

Figure S12 Cu K-edge XANES spectra collected under steady state conditions at 500 ^{o}C for O_2-activated monometallic (Cu-CZC) and bimetallic (Cu-Fe-mix) samples. The inset reports corresponding k^2-weighted FT-EXAFS amplitudes.

9 Additional XAS data

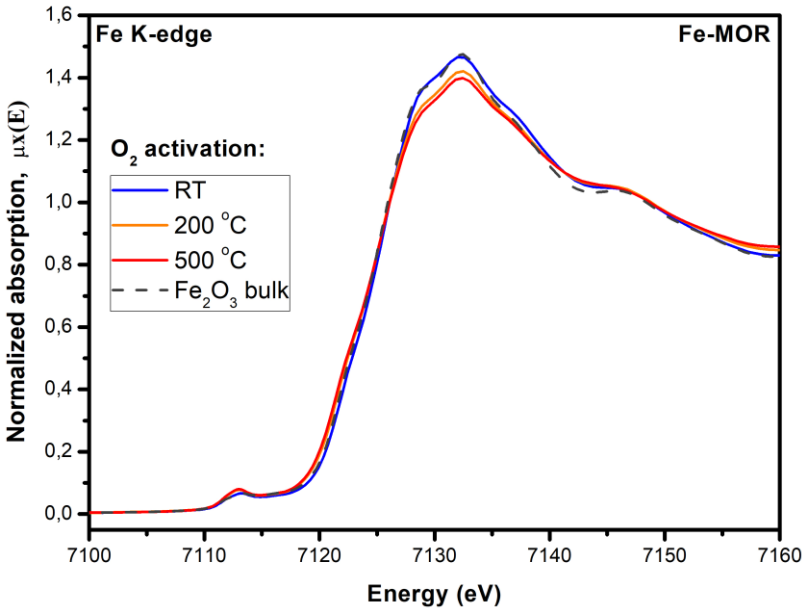

Figure S13 Fe K-edge XANES collected for monometallic Fe-MOR sample upon O_2-activation in comparison with the spectrum of reference compound - bulk α-Fe_2O_3.

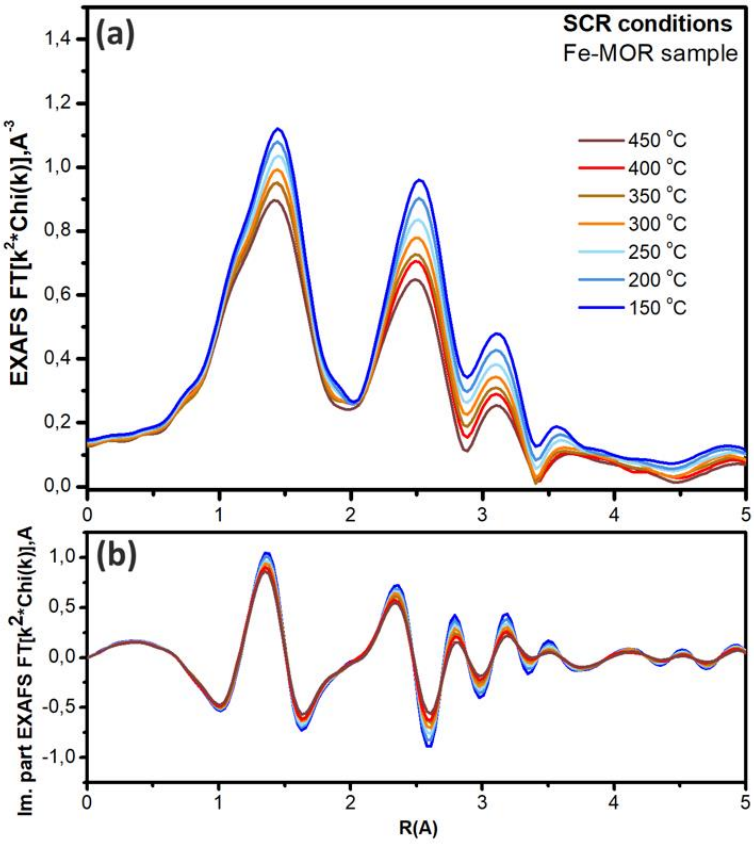

Figure S14 Fe K-edge k^2-weighted phase uncorrected FT-EXAFS **(a)** amplitudes and **(b)** imaginary parts collected for monometallic Fe-MOR samples under NH_3-SCR conditions.

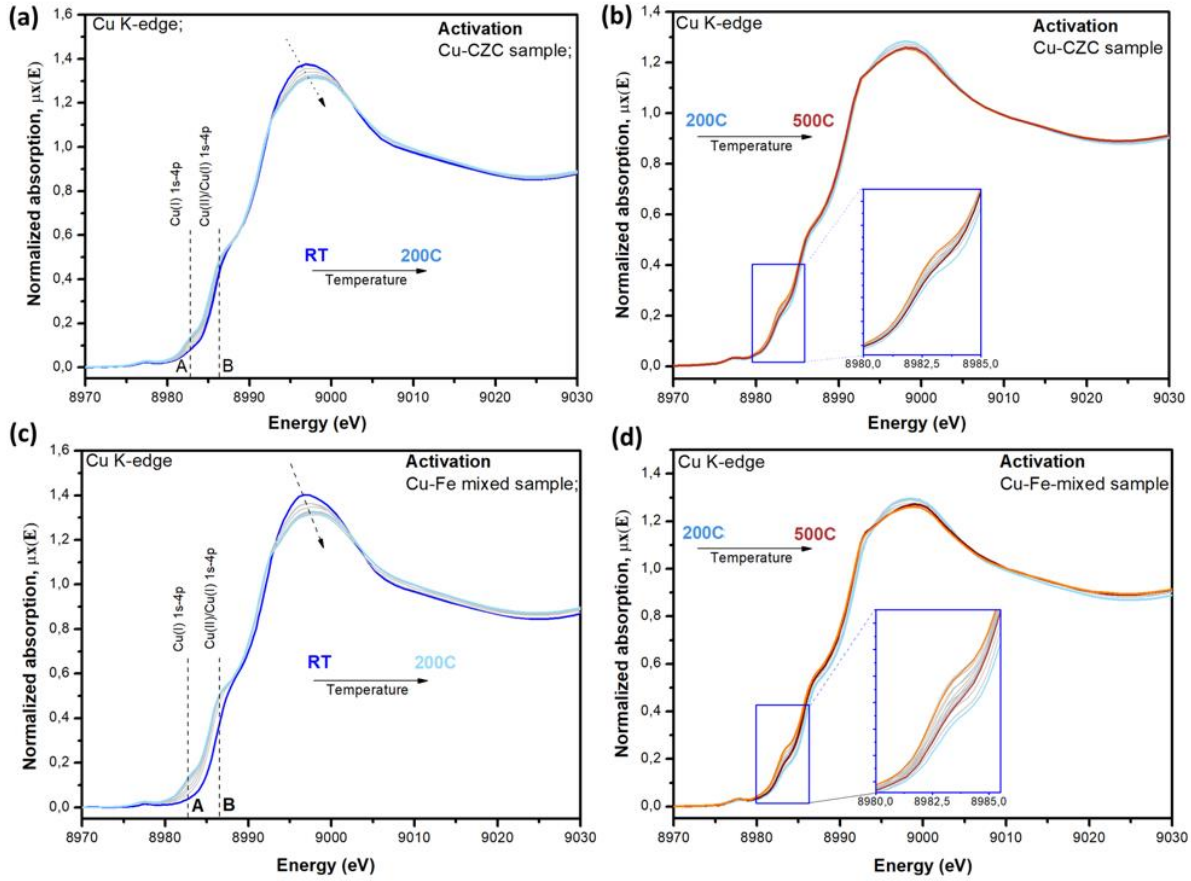

Figure S15 Cu K-edge XANES collected during temperature ramp upon activation in oxygen (10%O_2 + 90%He). Panels **(a,b)** and **(c,d)** represent the data collected for Cu-CZC and bimetallic Cu-Fe-mix samples, respectively. Panels **(a,c)** correspond to rehydration and the onset of transient auto-reduction stage, while panels **(b,d)** correspond to continuous transient auto-reduction and further re-oxidation stages. For panels **(b,d)** light blue curve correspond to dehydrated state, orange curve – auto-reduced state and dark red – re-oxidized state of the catalysts, while thin grey curves correspond to intermediate states.

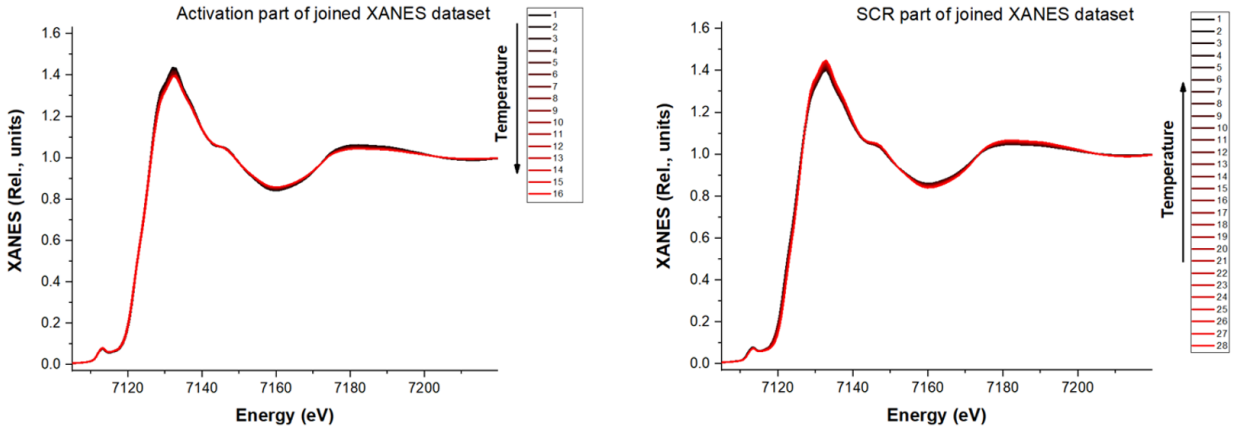

Figure S16 Activation and SCR parts of the Fe K-edge XANES dataset collected for F-MOR subjected for SVD decomposition procedure as described in Section 5.2 of SI.

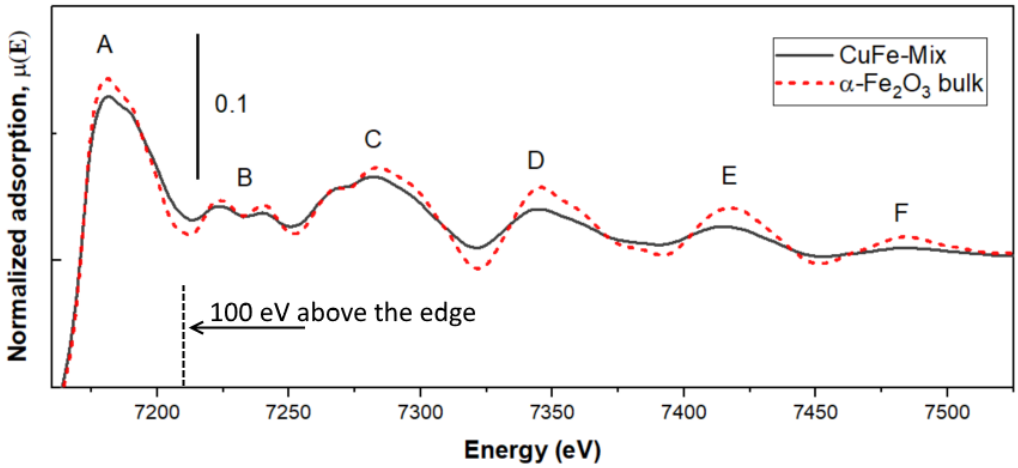

Figure S17 Magnified post-edge region of Fe K-edge normalized XANES spectra collected at RT for Cu-Fe-mix sample and reference material - bulk α-Fe_2O_3. The observed difference in the post-edge oscillations reveal strong size-effect for small Fe-O clusters formed in the CuFe-mixed catalyst.

References

[1] H.I. Hamoud, V. Valtchev, M. Daturi, Selective catalytic reduction of NO_x over Cu- and Fe-exchanged zeolites and their mechanical mixture, *Appl Catal B-Environ.*, **250** (2019) 419-428.

[2] L. Salassa, E. Borfecchia, T. Ruiu, C. Garino, D. Gianolio, R. Gobetto, P.J. Sadler, M. Cammarata, M. Wulff, C. Lamberti, Photo-Induced Pyridine Substitution in cis-$[Ru(bpy)_2(py)_2]Cl_2$: A Snapshot by Time-Resolved X-ray Solution Scattering, *Inorg. Chem.*, **49** (2010) 11240-11248.

[3] C. Prestipino, S. Bordiga, C. Lamberti, S. Vidotto, M. Garilli, B. Cremaschi, A. Marsella, G. Leofanti, P. Fisicaro, G. Spoto, A. Zecchina, Structural Determination of Copper Species on the Alumina-Supported Copper Chloride Catalyst: A Detailed EXAFS Study, *J. Phys. Chem. B* **107** (2003) 5022-5030.

[4] R.D. Horning, J.-L. Staudenmann, The Debye-Waller factor for polyatomic solids. Relationships between X-ray and specific-heat Debye temperatures. The Debye-Einstein model, *Acta Cryst. A*, **44** (1988) 136-142.

[5] P. Fornasini, R. Grisenti, On EXAFS Debye-Waller factor and recent advances, *J. Synchrot. Radiat.*, **22** (2015) 1242-1257.

[6] S. Calvin, S.X. Luo, C. Caragianis-Broadbridge, J.K. McGuinness, E. Anderson, A. Lehman, K.H. Wee, S.A. Morrison, L.K. Kurihara, Comparison of extended x-ray absorption fine structure and Scherrer analysis of X-ray diffraction as methods for determining mean sizes of polydisperse nanoparticles, *Appl. Phys. Lett.*, **87** (2005) 233102.

[7] S. Calvin, M.M. Miller, R. Goswami, S.-F. Cheng, S.P. Mulvaney, L.J. Whitman, V.G. Harris, Determination of crystallite size in a magnetic nanocomposite using extended x-ray absorption fine structure, *Int. J. Appl. Phys.*, **94** (2003) 778-783.

[8] A. Martini, S.A. Guda, A.A. Guda, G. Smolentsev, A. Algasov, O. Usoltsev, M.A. Soldatov, A. Bugaev, Y. Rusalev, C. Lamberti, A.V. Soldatov, PyFitit: The software for quantitative analysis of XANES spectra using machine-learning algorithms, *Comput. Phys. Commun.*, **250** (2019) 107064.

[9] R.G. Brereton, Chemometrics: data analysis for the laboratory and chemical plant, John Wiley & Sons 2003.

[10] E.R. Malinowski, Factor analysis in chemistry, Wiley2002.

[11] M. Fernandez Garcia, C.M. Alvarez, G.L. Haller, XANES-TPR study of Cu-Pd bimetalic catalysts - application of factor analysis *J. Phys. Chem.*, **99** (1995) 12565-12569.

[12] A. Manceau, M. Marcus, T. Lenoir, Estimating the number of pure chemical components in a mixture by X-ray absorption spectroscopy, *J. Synchrot. Radiat.*, **21** (2014) 1140-1147.

[13] A. de Juan, J. Jaumot, R. Tauler, Multivariate Curve Resolution (MCR). Solving the mixture analysis problem, *Anal. Methods*, **6** (2014) 4964-4976.

[14] S.C. Rutan, A. de Juan, R. Tauler, 2.06 - Introduction to Multivariate Curve Resolution☆, in: S. Brown, R. Tauler, B. Walczak (Eds.) Comprehensive Chemometrics (Second Edition), Elsevier, Oxford, 2020, pp. 85-94.
[15] A. Martini, E. Borfecchia, K.A. Lomachenko, I.A. Pankin, C. Negri, G. Berlier, P. Beato, H. Falsig, S. Bordiga, C. Lamberti, Composition-driven Cu-speciation and reducibility in Cu-CHA zeolite catalysts: a multivariate XAS/FTIR approach to complexity, *Chem. Sci*., **8** (2017) 6836-6851.
[16] E. Borfecchia, C. Negri, K.A. Lomachenko, C. Lamberti, T.V.W. Janssens, G. Berlier, Temperature-dependent dynamics of NH_3-derived Cu species in the Cu-CHA SCR catalyst, *React. Chem. Eng*., **4** (2019) 1067-1080.
[17] W. Windig, J. Guilment, Interactive self-modeling mixture analysis, *Anal. Chem*., **63** (1991) 1425-1432.
[18] E. Borfecchia, K.A. Lomachenko, F. Giordanino, H. Falsig, P. Beato, A.V. Soldatov, S. Bordiga, C. Lamberti, Revisiting the nature of Cu sites in the activated Cu-SSZ-13 catalyst for SCR reaction, *Chem. Sci*., **6** (2015) 548-563.
[19] T.V.W. Janssens, H. Falsig, L.F. Lundegaard, P.N.R. Vennestrøm, S.B. Rasmussen, P.G. Moses, F. Giordanino, E. Borfecchia, K.A. Lomachenko, C. Lamberti, S. Bordiga, A. Godiksen, S. Mossin, P. Beato, A Consistent Reaction Scheme for the Selective Catalytic Reduction of Nitrogen Oxides with Ammonia, *ACS Catal.*, **5** (2015) 2832-2845.
[20] C. Tyrsted, E. Borfecchia, G. Berlier, K.A. Lomachenko, C. Lamberti, S. Bordiga, P.N.R. Vennestrøm, T.V.W. Janssens, H. Falsig, P. Beato, A. Puig-Molina, Nitrate–nitrite equilibrium in the reaction of NO with a Cu-CHA catalyst for NH_3-SCR, *Catal. Sci. Technol*., **6** (2016) 8314-8324.
[21] C. Negri, E. Borfecchia, M. Cutini, K.A. Lomachenko, T.V.W. Janssens, G. Berlier, S. Bordiga, Cover Feature: Evidence of Mixed-Ligand Complexes in Cu−CHA by Reaction of Cu Nitrates with NO/NH3 at Low Temperature (ChemCatChem 16/2019), *ChemCatChem*, **11** (2019) 3555-3555.
[22] F. Giordanino, E. Borfecchia, K.A. Lomachenko, A. Lazzarini, G. Agostini, E. Gallo, A.V. Soldatov, P. Beato, S. Bordiga, C. Lamberti, Interaction of NH_3 with Cu-SSZ-13 catalyst: A complementary FTIR, XANES, and XES study, *J. Phys. Chem. Lett.*, **5** (2014) 1552-1559.
[23] K.A. Lomachenko, E. Borfecchia, C. Negri, G. Berlier, C. Lamberti, P. Beato, H. Falsig, S. Bordiga, The Cu-CHA deNOx Catalyst in Action: Temperature-Dependent NH_3-Assisted Selective Catalytic Reduction Monitored by Operando XAS and XES, *J. Am. Chem. Soc.*, **138** (2016) 12025-12028.
[24] L. Chen, T.V.W. Janssens, M. Skoglundh, H. Grönbeck, Interpretation of NH_3-TPD profiles from Cu-CHA using First-Principles calculations, *Top. Catal.*, **62** (2019) 93-99.
[25] G. te Velde, F.M. Bickelhaupt, E.J. Baerends, C. Fonseca Guerra, S.J.A. van Gisbergen, J.G. Snijders, T. Ziegler, Chemistry with ADF, *J. Comput. Chem.*, **22** (2001) 931-967.
[26] P. Frank, M. Benfatto, B. Hedman, K.O. Hodgson, Solution $[Cu(amm)]^{2+}$ is a Strongly Solvated Square Pyramid: A Full Account of the Copper K-edge XAS Spectrum Within Single-Electron Theory, *Inorg. Chem*., **47** (2008) 4126-4139.
[27] D.K. Pappas, E. Borfecchia, M. Dyballa, I.A. Pankin, K.A. Lomachenko, A. Martini, M. Signorile, S. Teketel, B. Arstad, G. Berlier, C. Lamberti, S. Bordiga, U. Olsbye, K.P. Lillerud, S. Svelle, P. Beato, Methane to methanol: Structure activity relationships for Cu-CHA, *J. Am. Chem. Soc*., **139** (2017) 14961-14975.
[28] I.A. Pankin, A. Martini, K.A. Lomachenko, A.V. Soldatov, S. Bordiga, E. Borfecchia, Identifying Cu-oxo species in Cu-zeolites by XAS: A theoretical survey by DFT-assisted XANES simulation and EXAFS wavelet transform, *Catal. Today*, **345** (2020) 125-135.
[29] R. L. Blake, R.E. Hessevick, T. Zoltai, L. W. Finger, *Am. Mineral.*, **51**, (1966), 123-129
[30] C. Negri, E. Borfecchia, A. Martini, G. Deplano, K.A. Lomachenko, T. V.W. Janssens, G. Berlier and S. Bordiga, *Res. Chem. Intermed*, accepted, DOI: 10.1007/s11164-020-04350-1